Using Targeted Phonon Excitation to Modulate Thermal Conductivity of Boron Nitride

Dongkai Pan(潘东楷)[1], Tianhao Li(李天豪)[1,2], Xiao Wan(万骁)[1], Zhicheng Zong(宗志成)[1,2], Yangjun Qin(秦杨军)[1,2], and Nuo Yang(杨诺)[2*]

[1]*School of Energy and Power Engineering, Huazhong University of Science and Technology, Wuhan 430074, China*
[2]*Department of Physics, National University of Defense Technology, Changsha 410073, China*

(Received 20 March 2025; accepted manuscript online 16 May 2025)

Recent advancements in thermal conductivity modulating strategies have shown promising enhancements to the thermal management capabilities of two-dimensional materials. In this article, both the iterative Boltzmann transport equation solution and the two-temperature model were employed to investigate the efficacy of targeted phonon excitation applied to hexagonal boron nitride (hBN). The results indicate significant modifications to hBN's thermal conductivity, achieving increases of up to 30.1% as well as decreases of up to 59.8%. These findings validate the reliability of the strategy, expand its scope of applicability, and establish it as a powerful tool for tailoring thermal properties across a wider range of fields.

DOI: 10.1088/0256-307X/42/7/070801 CSTR: 32039.14.0256-307X.42.7.070801

Thermal conductivity is a critical property with significant implications across various applications. The requirements for thermal conductivity vary depending on specific circumstances. In thermal management, high thermal conductivity is essential for efficient heat dissipation to prevent device overheating and ensure reliability.[1] Conversely, in thermoelectric applications, low thermal conductivity is preferred to achieve a high figure of merit (zT) and enhance thermoelectric performance.[2–4] These contrasting demands underscore the importance of effective modulation techniques.[5] Phonon transport predominantly governs heat conduction in most semiconductors; thus, phonon-based modulation strategies are extensively researched.

There are numerous physical mechanisms influencing phonon transport and offering pathways for modulation.[5–7] For instance, thermal conductivity can be enhanced by minimizing phonon–phonon scattering phase space and reducing phonon–impurity scattering rates, as observed in materials like cubic boron arsenide and low-dimensional materials.[8–13] Conversely, larger anharmonicity, increased crystal complexity, or additional scattering sources such as disorder and interfaces can reduce thermal conductivity by enhancing scattering strength.[14–17] Beyond scattering mechanisms, other physical mechanisms, such as phonon resonance hybridization, coherent regimes, phase transitions, and localization mechanisms, are also promising avenues for modulation.[18–25] The strength of interactions also significantly impacts thermal conductivity,[26–31] while external factors such as electric fields and external pressure show potential for modulation as well.[26,32,33] However, regulatory strategies generally rely on introducing structural changes or specific nanostructures to modulate phonon transport, leading to irreversible alterations in material structures.

Inspired by the phonon weak coupling mechanism[34–37] and the realization of phonon modes excitation in experiments,[38–40] a novel modulation approach utilizing targeted phonon excitation to modulate thermal conductivity has been proposed recently.[41] In low-dimensional systems, phonon–phonon interactions are much weaker compared to those observed in conventional bulk materials. This attenuation in interactions is also known as phonon weak coupling. The weak coupling mechanism limits the energy exchange between phonon modes, thereby facilitating the thermal conductivity modulation based on selective modal excitation. This method enables reversible *in situ* dynamic modulation by regulating the phonon distribution function through selective energy injection, without altering the intrinsic material structure. Its efficacy has been validated on graphene, which has a super high thermal conductivity, through *ab initio* calculations and molecular dynamics simulations. Moreover, results on other materials are crucial for the demonstration of its broader applicability. Here, hexagonal boron nitride (hBN) is chosen as the platform due to its widespread use as an encapsulation material and its notably lower thermal conductivity compared to graphene, despite both being two-dimensional (2D) phonon weak coupling systems.

In this work, the effect of targeted phonon excitation on thermal conductivity modulation is further explored on hBN. Initially, the phonon density of states (DOS), scattering rates, and spectral mapping of thermal conductivity are calculated as a guidance for subsequent exci-

*Corresponding author. Email: nuo@nudt.edu.cn
© 2025 Chinese Physical Society and IOP Publishing Ltd. All rights, including for text and data mining, AI training, and similar technologies, are reserved.

tation and modulation. Based on the interplay between various mechanisms, the modulation results are first predicted qualitatively and then validated against the calculated outcomes. Two methods are employed to calculate post-excitation modulation thermal conductivity: iterative Boltzmann transport equation (BTE) solution [42] and two-temperature model (TTM). [34] The results from the two methods are compared to ensure their consistency. In this way, the effectiveness of the modulation strategy is validated on hBN.

The modulating outcome hinges on the selection of targeted phonon modes, with a focus on their participation in heat conduction. Several key parameters, such as scattering rates, spectral thermal conductivity, and phonon DOS, are chosen to characterize the involvement of the phonon modes within specific frequency ranges in the heat conducting process.

Scattering rate serves as a fundamental metric in estimating the resistance in transport processes, where a higher scattering rate generally indicates worse transport properties. Modes with high scattering rates are prioritized in modulation aimed at reducing thermal conductivity, as their excitation tends to adversely affect other modes.

Additionally, modulation targets all modes within certain frequency ranges rather than targeting individual modes, due to the dense distribution of modes and the difficulty in selectively exciting one mode. In this case, spectral mapping of thermal conductivity is utilized to represent the contribution of modes across different frequency ranges to heat conduction. The modes within frequency ranges exhibiting higher spectral thermal conductivity are leveraged to enhance thermal conductivity.

What is more, while the phonon DOS is not directly related to the phonon transport process, it dictates the number of modes within unit frequency intervals, thus determining the number of modes for excitation. In other words, a higher DOS signifies more modes within corresponding frequency ranges, which can lead to more significant effects on thermal conductivity, regardless of whether the overall impact is positive or negative.

Building upon the established modulation principles, the computation details are presented below. A $5\times5\times1$ supercell was constructed for the calculation of second- and third-order force constants. The second-order force constants were obtained via density functional perturbation theory, implemented by the Vienna *ab initio* simulation package (VASP). [43,44] In the calculation of second-order force constants, a comparison was made between density functional perturbation theory and the finite displacement method, with no observable differences between them. The third-order force constants were calculated using the finite displacement method, and the cutoff radius for the calculation of third-order force constants was set to the 6th nearest neighbor.

The overall thermal conductivity is calculated via the iterative solution of linearized phonon BTE with a Γ-centered $50\times50\times1$ regular grid at a temperature of 300 K (a temperature of 300 K is assumed throughout this paper unless otherwise specified). Modulation is implemented by introducing a multiplier N to the phonon distribution function f within the selected frequency ω, as expressed as

$$f(\omega) = \frac{N}{\exp(\hbar\omega/k_{\mathrm{B}}T) - 1}. \tag{1}$$

This modification is incorporated into the ShengBTE code [45] to realize the excitation of targeted phonon modes. The incorporation is achieved by inserting the multiplied distribution function into the calculations of scattering rates and heat capacity. To illustrate this approach, the formula for calculating three-phonon scattering rates for emission processes is presented as

$$\Gamma^{-}_{\lambda\lambda'\lambda''} = \frac{\hbar\pi}{4}\frac{f'_0 + f''_0 + 1}{\omega_\lambda\omega_{\lambda'}\omega_{\lambda''}}|V^{-}_{\lambda\lambda'\lambda''}|^2\delta(\omega_\lambda - \omega_{\lambda'} - \omega_{\lambda''}), \tag{2}$$

where λ, λ', and λ'' denote the three phonon modes involved in the three-phonon scattering process. Here, f'_0 stands for $f_0(\omega_{\lambda'})$ and so forth. $V^{-}_{\lambda\lambda'\lambda''}$ is the scattering matrix element (the superscript "$-$" represents emission process), which is determined by material's intrinsic properties. Here, a specialized version of ShengBTE developed by Ruan *et al.* [46] is utilized as the baseline for its enhanced convergence performance on 2D materials. The consideration of anharmonicity is up to the third order.

Given the nonequilibrium state induced by phonon mode excitation, defining temperatures for the targeted modes specifically becomes challenging. Here, the concept of an "effective temperature T'" for the phonon mode is introduced. This temperature is derived from the post-excitation modal energy E_ω via the Bose–Einstein distribution:

$$T' = \frac{\hbar\omega}{k_{\mathrm{B}}}\ln^{-1}\left(\frac{\hbar\omega}{E_\omega} + 1\right). \tag{3}$$

Based on this effective temperature T', adjustments are made to the heat capacity calculation. Conventionally, heat capacity calculation relies on the derivative of the phonon distribution function with respect to temperature. The heat capacity is corrected using T' defined in Eq. (3) to more accurately reflect the system's thermodynamic properties under excitation.

As to the TTM, it is well-suited for describing non-equilibrium conditions between different phonon groups in weak coupling systems, encompassing interactions such as electron–phonon and phonon–phonon couplings. [34,35,47,48] In the TTM framework, the excited phonon group and other intrinsic phonon groups are treated separately, and the non-equilibrium is assumed to exist mainly between the two groups due to their weak coupling. The TTM model parameterizes the weak coupling between the two phonon groups with the coupling coefficient $G_{\mathrm{ex,in}}$, defined as

$$G_{\mathrm{ex,in}} = \frac{c_{\mathrm{ex}}c_{\mathrm{in}}}{\tau_{\mathrm{ex,in}}(c_{\mathrm{ex}} + c_{\mathrm{in}})}, \tag{4}$$

where c_{ex} and c_{in} denote the specific heat capacities of the excited and intrinsic phonons, respectively, and $\tau_{\mathrm{ex,in}}$ represents the relaxation time for the coupling between the two phonon groups. The equivalent thermal conductivity

κ of the system within the TTM framework is expressed as

$$\kappa = \frac{\kappa_{\rm ex} + \kappa_{\rm in}}{1 - \left[\frac{c_{\rm ex}}{c_{\rm ex}+c_{\rm in}} - \frac{c_{\rm in}\kappa_{\rm ex}}{(c_{\rm ex}+c_{\rm in})\kappa_{\rm in}}\right] {\rm e}^{-\gamma x}}, \tag{5}$$

where $\gamma = \sqrt{G_{\rm ex,in}(1/\kappa_{\rm ex} + 1/\kappa_{\rm in})}$, x represents the characteristic size of the system, and $\kappa_{\rm ex}$ and $\kappa_{\rm in}$ represent the thermal conductivity of excited and intrinsic phonons, respectively.

By utilizing two distinct approaches, the robustness and accuracy of the results could be increased. As will be revealed in the results section, the results from the two parallel approaches show good consistency and demonstrate the great modulation effect of the strategy.

The scattering rates and density of states of phonon modes in hBN are calculated as a reference for further modulation. The results depicted in Fig. 1 reveal two features. Firstly, the scattering rates of ZA modes exhibit a gradual increase with frequency until reaching the top of the ZA branch, which is also the first peak (Van Hove singularity) in phonon DOS. This indicates the potential of the ZA modes near the top of the ZA branch for modulation aimed at reducing thermal conductivity. Secondly, the maximum scattering rate occurs near the second peak of phonon DOS, indicating that the modes around this frequency can also be utilized to lower the thermal conductivity. Despite the highest peak of phonon DOS falling within the range of optical branches, these modes contribute little to thermal conductivity due to their low group velocity.

The spectral mapping of thermal conductivity in hBN is calculated by differentiating the cumulative thermal conductivity, as shown in Fig. 2. The contribution from low-frequency modes is surpassing compared to others, indicating the great potential of these modes for enhancing thermal conductivity. This suggests that these modes are the primary contributor to thermal conductivity. Therefore, by exciting the modes within this range, the thermal conduction with BN is supposed to be increased. At the same time, considering the scattering rates and phonon DOS in Fig. 1, it is noted that the low phonon DOS near the point imposes limitations on the enhancement. Consequently, the peak for the final enhancing modulation in heat conduction should be located slightly away from the point to allow for higher phonon DOS and enough spectral mapping of thermal conductivity. Following the peak, the spectral mapping of thermal conductivity declines sharply while scattering rates increase rapidly. This causes the enhancing modulating effect to diminish fast and soon transitions to a reducing effect, which continues to intensify until the formation of a trough corresponding to the phonon DOS peak at the top of the ZA branch (around 9 THz).

A similar situation is also observed at higher frequency around 18 THz, where the scattering is much stronger and spectral mapping of thermal conductivity is limited due to lower group velocity. So, the phonon DOS in this region also brings a modulation trough. As for higher optical modes, the extremely low spectral mapping of thermal conductivity of optical modes again validates their negligible contribution to thermal conductivity, so the excitation targeting them should cause no significant effect.

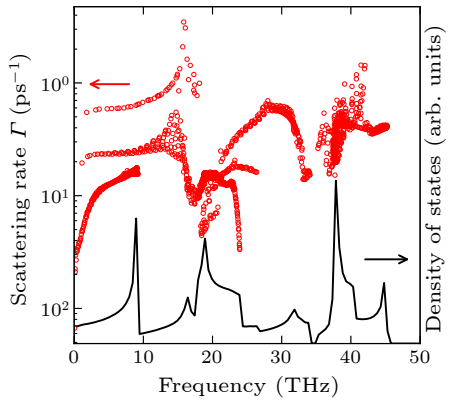

Fig. 1. The scattering rates Γ (red circles) and phonon DOS (black line) of hBN.

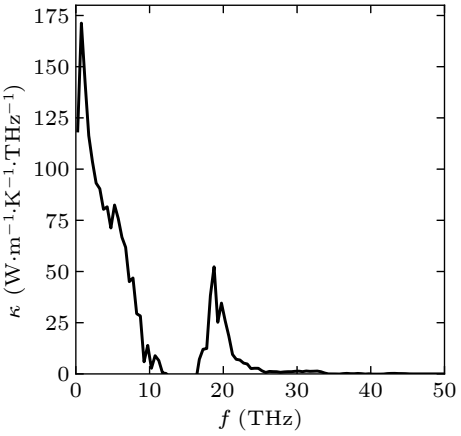

Fig. 2. The spectral mapping of thermal conductivity in hBN. The value represents the contribution of the modes of certain frequencies to thermal conductivity. The overall thermal conductivity is 885 W·m^{-1}·K^{-1}.

Based on the above theoretical analysis, it is predicted that there will be one peak (enhancement) and two troughs (reduction) in the spectra. The peak is located close to the Γ point. Meanwhile, the first trough corresponds to the top of the ZA branch, and the second trough lies around the second peak of phonon DOS. These predictions will be validated using the subsequent calculation results.

The modulation results under different multipliers are demonstrated in Fig. 3(a). The relative thermal conductivity κ/κ_0 is the ratio of post-exciting thermal conductivities κ to the intrinsic one κ_0. By comparing the modulation results with multiplier 5 (blue squares) and multiplier 25 (orange circles), it is evident that only the amplitudes of the modulation differ, while the qualitative performance remains consistent. This confirms the robustness of this modulation strategy. Besides, in Fig. 3(b), by comparing the calculation results of iterative BTE (orange circles) and the TTM (blue triangles), it is found that the two methods are highly consistent. This further verifies the reliability of the results.

It is clearly demonstrated that there are one peak and two troughs in the results, consistent with the theoretical prediction above. The peak is located at 1.45 THz (exciting the modes within 1.4–1.5 THz), while the troughs

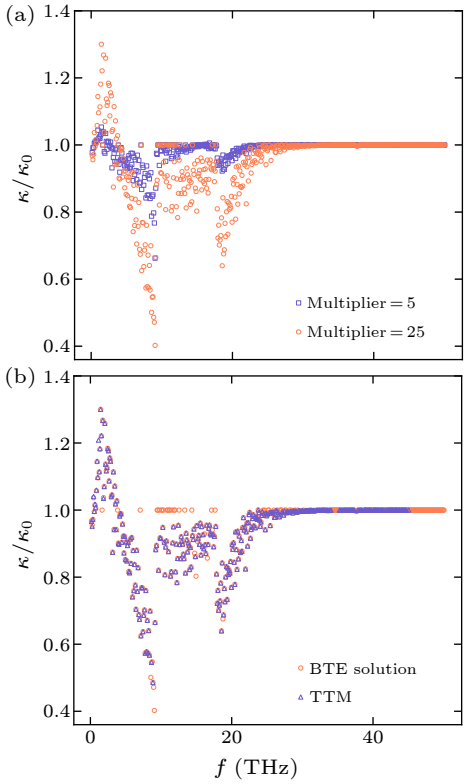

Fig. 3. Relative overall thermal conductivity of hBN (κ/κ_0) versus the center frequency of the excited targeted phonons. (a) Results for different multipliers. (b) Results calculated from TTM as well as iterative BTE solution when the multiplier is set to 25. Each point in the diagram represents one modulation result. For instance, the first point is located at 0.05 THz, meaning modes in 0–0.1 THz are excited with 5 or 25 times larger energy, depending on the multiplier.

are located at 9.05 THz and 18.55 THz, respectively. The peak arises from the combined effect of the dominating spectral mapping of thermal conductivity and increasing phonon DOS. The troughs result from the sharp DOS peaks and high scattering rates.

To demonstrate the feasibility of the strategy, an estimate of the energy needed for excitation is made. When the multiplier is set to 25 and phonon modes within the 1.4–1.5 THz range are targeted, the required energy density is approximately 1.6 $\mathrm{J{\cdot}m^{-2}}$, which is comparable to the typical energy densities achieved in experimental setups.[49]

Moreover, the same pattern, containing one peak and two troughs, exists similarly in the results on graphene.[41] This similarity arises from the common features of 2D phonon weak coupling systems, where interactions between in-plane and out-of-plane phonon modes are significantly weaker than in most bulk materials. The weak coupling restricts energy exchange between these phonon modes, thereby reducing energy dissipation and enabling targeted excitation of specific modes. Additionally, the highly similar crystal structures of hBN and graphene lead to comparable phonon dispersion, further reinforcing the similarity.

To conclude, thermal conductivity modulation based on targeted phonon excitation is further validated by iterative BTE solution and TTM on hBN. The selection of targeted phonon modes is based on a comprehensive consideration of phonon DOS, scattering rate, as well as spectral mapping of thermal conductivity. The consistent results from both parallel methods demonstrate the validity of the modulation on hBN. The results show that thermal conductivity modulation on hBN can achieve up to a 30.1% increase and a 59.8% decrease.

These findings underscore the reliability of the strategy. The similar pattern observed in different materials suggests that this modulation strategy has broad applicability across different materials, which will provide a fantastic *in situ* way to manipulate thermal conductivity. Moreover, such a quantum-level modulation can provide an excellent platform for the observation of the response of macroscopic properties like thermal conductivity to microscopic perturbations. By enabling precise control over thermal conductivity at the quantum level, the strategy could significantly improve thermal management in electronic devices, enhance the efficiency of thermoelectric materials, and contribute to the development of next-generation heat control technologies.

The data that support the findings of this study are available from the corresponding author upon reasonable request.

Acknowledgements. The work was supported by the National Key Research and Development Project of China (Grant No. 2018YFE0127800). This work was carried out at the National Supercomputer Center in Tianjin, and the calculations were performed on TianHe-HPC.

References

[1] Song H, Liu J, Liu B, Wu J, Cheng H M, and Kang F 2018 *Joule* **2** 442
[2] Chen G, Zeng T, Borca-Tasciuc T, and Song D 2000 *Mater. Sci. Eng. A* **292** 155
[3] Snyder G J and Toberer E S 2008 *Nat. Mater.* **7** 105
[4] Ji R C, Peng G L, Xu Z W, Yang N, and Hao Q 2022 *ACTA Phys. Sin.* **71** 168401 (in Chinese)
[5] Qian X, Zhou J, and Chen G 2021 *Nat. Mater.* **20** 1188
[6] Li N, Ren J, Wang L, Zhang G, Hänggi P, and Li B 2012 *Rev. Mod. Phys.* **84** 1045
[7] Ding Y F, Zhu G M, Shen X Y, Bai X, and Li B W 2022 *Chin. Phys. B* **31** 126301
[8] Kang J S, Li M, Wu H, Nguyen H, and Hu Y 2018 *Science* **361** 575
[9] Tian F, Song B, Chen X, Ravichandran N K, Lv Y C, Chen K, Sullivan S, Kim J, Zhou Y Y, Liu T H, Goni M, Ding Z W, Sun J Y, Gamage U A G, Sun H, Ziyaee H, Huyan S, Deng L, Zhou J, Schmidt A J, Chen S, Chu C W, Huang P Y, Broido D, Shi L, Chen G, and Ren Z F 2018 *Science* **361** 582
[10] Li S, Zheng Q, Lv Y, Liu X, Wang X, Huang P Y, Cahill D G, and Lv B 2018 *Science* **361** 579
[11] van Roekeghem A, Carrete J, Oses C, Curtarolo S, and Mingo N 2016 *Phys. Rev. X* **6** 041061
[12] Lindsay L and Broido D A 2008 *J. Phys. Condens. Matter* **20** 165209
[13] Lindsay L, Broido D A, and Mingo N 2010 *Phys. Rev. B* **82** 115427

[14] Kim W, Zide J, Gossard A, Klenov D, Stemmer S, Shakouri A, and Majumdar A 2006 *Phys. Rev. Lett.* **96** 045901
[15] Poudel B, Hao Q, Ma Y, Lan Y, Minnich A, Yu B, Yan X, Wang D Z, Muto A, Vashaee D, Chen X Y, Liu J M, Dresselhaus M S, Chen G, and Ren Z F 2008 *Science* **320** 634
[16] Yang Y, Ma D K, and Zhang L F 2023 *Chin. Phys. Lett.* **40** 124401
[17] Wu K F, Zhang H, and Tang G H 2024 *Chin. Phys. Lett.* **41** 034401
[18] Luckyanova M N, Garg J, Esfarjani K, Jandl A, Bulsara M T, Schmidt A J, Minnich A J, Chen S, Dresselhaus M S, Ren Z F, Fitzgerald E A, and Chen G 2012 *Science* **338** 936
[19] Ravichandran J, Yadav A K, Cheaito R, Rossen P B, Soukiassian A, Suresha S J, Duda J C, Foley B M, Lee C H, Zhu Y, Lichtenberger A W, Moore J E, Muller D A, Schlom D G, Hopkins P E, Majumdar A, Ramesh R, and Zurbuchen M A 2014 *Nat. Mater.* **13** 168
[20] Davis B L and Hussein M I 2014 *Phys. Rev. Lett.* **112** 055505
[21] Ma D, Ding H, Meng H, Feng L, Wu Y, Shiomi J, and Yang N 2016 *Phys. Rev. B* **94** 165434
[22] Wan X, Ma D, Pan D, Yang L, and Yang N 2021 *Mater. Today Phys.* **20** 100445
[23] Meng H, Maruyama S, Xiang R, and Yang N 2021 *Int. J. Heat Mass Transf.* **180** 121773
[24] Zhang Z, Guo Y, Bescond M, Chen J, Nomura M, and Volz S 2022 *Phys. Rev. Lett.* **128** 015901
[25] Zhang D, Ren W, Wang K, Chen S, Zhang L, Ni Y, and Zhang G 2023 *Chin. Phys. B* **32** 050505
[26] Deng S, Ma D, Zhang G, and Yang N 2021 *J. Mater. Chem. A* **9** 24472
[27] Yu X, Ma D, Deng C, Wan X, An M, Meng H, Li X, Huang X, and Yang N 2021 *Chin. Phys. Lett.* **38** 014401
[28] Dong L, Liu B, Wang Y, and Xu X 2022 *Chin. Phys. Lett.* **39** 127201
[29] Qiu R, Zeng Q Y, Wang H, Kang D D, Yu X X, and Dai J Y 2023 *Chin. Phys. Lett.* **40** 116301
[30] Lou Q and Xia M G 2023 *Chin. Phys. Lett.* **40** 094401
[31] Liu Y Z, Yue J C, Liu Y N, Nian L L, and Hu S Q 2023 *Chin. Phys. Lett.* **40** 086301
[32] Deng S, Yuan J, Lin Y, Yu X, Ma D, Huang Y, Ji R, Zhang G, and Yang N 2021 *Nano Energy* **82** 105749
[33] Zhou Y, Dong Z Y, Hsieh W P, Goncharov A F, and Chen X J 2022 *Nat. Rev. Phys.* **4** 319
[34] An M, Song Q, Yu X, Meng H, Ma D, Li R, Jin Z, Huang B, and Yang N 2017 *Nano Lett.* **17** 5805
[35] Deng C, Huang Y, An M, and Yang N 2021 *Mater. Today Phys.* **16** 100305
[36] Pan D K, Zong Z C, and Yang N 2022 *Acta Phys. Sin.* **71** 086302 (in Chinese)
[37] Chen J, He J, Pan D, Wang X, Yang N, Zhu J, Yang S A, and Zhang G 2022 *Sci. China Phys. Mech. Astron.* **65** 117002
[38] Wu X, Néel N, Brandbyge M, and Kröger J 2023 *Phys. Rev. Lett.* **130** 116201
[39] Sekiguchi F, Hirori H, Yumoto G, Shimazaki A, Nakamura T, Wakamiya A, and Kanemitsu Y 2021 *Phys. Rev. Lett.* **126** 077401
[40] Yoon Y, Lu Z, Uzundal C, Qi R, Zhao W, Chen S, Feng Q, Kim W, Naik M H, Watanabe K, Taniguchi T, Louie S G, Crommie M F, and Wang F 2024 *Nature* **631** 771
[41] Wan X, Zong Z, Qin Y, Lü J T, Volz S, Zhang L, and Yang N 2024 *Nano Lett.* **24** 6889
[42] Omini M and Sparavigna A 1995 *Phys. B Condens. Matter* **212** 101
[43] Kresse G and Furthmüller J 1996 *Phys. Rev. B* **54** 11169
[44] Kresse G and Furthmüller J 1996 *Comput. Mater. Sci.* **6** 15
[45] Li W, Carrete J, A. Katcho N, and Mingo N 2014 *Comput. Phys. Commun.* **185** 1747
[46] Han Z, Yang X, Li W, Feng T, and Ruan X 2022 *Comput. Phys. Commun.* **270** 108179
[47] Majumdar A and Reddy P 2004 *Appl. Phys. Lett.* **84** 4768
[48] Liao B, Zhou J, and Chen G 2014 *Phys. Rev. Lett.* **113** 025902
[49] Sekiguchi F, Hirori H, Yumoto G, Shimazaki A, Nakamura T, Wakamiya A, and Kanemitsu Y 2021 *Phys. Rev. Lett.* **126** 077401